CrystEngComm

ROYAL SOCIETY OF CHEMISTRY

PAPER

View Article Online
View Journal | View Issue

Cite this: *CrystEngComm*, 2022, **24**, 3972

Hydrothermal formation of bismuth-titanate nanoplatelets and nanowires: the role of metastable polymorphs†

Darko Makovec, *[ab] Nina Križaj[ab] and Sašo Gyergyek [a]

Understanding the processes involved in the formation of nanoparticles is a prerequisite for the control of their morphology. In this investigation we reveal the processes leading to the formation of two distinct morphologies of bismuth-titanate ($Bi_4Ti_3O_{12}$) nanoparticles, *i.e.*, nanoplatelets and nanowires, during hydrothermal treatment of precipitated Bi^{3+} and Ti^{4+} ions in a mineralizer hydroxide aqueous solution. Washed precipitates of the two ions in a stoichiometric ratio were suspended in hydroxide (NaOH or KOH) and hydrothermally treated for different times at temperatures up to 220 °C. The product was analysed with a combination of X-ray diffractometry and different electron-microscopy techniques using a transmission and an aberration-corrected scanning-transmission electron microscope. The hydrothermal treatment for 38 hours at 200 °C led to the formation of nanowires with a metastable orthorhombic structure and nanoplatelets with an equilibrium Aurivillius layered-perovskite structure at lower (≤1 mol L^{-1}) and higher (>1 mol L^{-1}) NaOH concentrations, respectively. At the initial stage of the hydrothermal synthesis, a mixture of two metastable polymorphs was formed: the nanowires and the highly defective perovskite phase. The perovskite phase in the form of globular aggregates of nanocrystallites only contained Bi^{3+} and Ti^{4+} cations (Na^+, K^+ and Ti^{3+} were not detected). In the continuation of the hydrothermal treatment, the aggregates of perovskite nanocrystals dissolved at lower NaOH concentrations, whereas at higher NaOH concentrations the nanowires dissolved while the Aurivillius nanoplatelets grew from the surfaces of the perovskite aggregates.

Received 7th April 2022,
Accepted 21st April 2022

DOI: 10.1039/d2ce00491g

rsc.li/crystengcomm

Introduction

Ferroelectric nanoparticles are becoming increasingly important because of their potential in advanced applications, such as non-volatile random-access-memory devices,[1] nanogenerators for biomechanical energy harvesting,[2] for tuneable electro-optical materials, *e.g.*, in liquid-crystal dispersions,[3] in biomedicine, *e.g.*, for second harmonic generation imaging,[4] and for different sensing applications.[5,6] Using different wet-chemical methods, nanoparticles of different ferroelectric materials have been synthesized. The main challenge in the synthesis of the nanoparticles remains the control of their morphology needed to fulfil the requirements of a specific application. The hydrothermal method has proven to be a simple and versatile way to synthesise ferroelectric bismuth-titanate nanoparticles with a rich variety of different morphologies.[5–16] During the hydrothermal treatment of Bi and Ti hydroxides, bismuth titanate (BIT, $Bi_4Ti_3O_{12}$) forms at moderate concentrations of mineralizer hydroxide (NaOH or KOH), whereas at higher concentrations of the mineralizer a mixed, sodium/potassium bismuth titanate ($Bi_{0.5}(Na/K)_{0.5}TiO_3$) perovskite is formed.[9,17] BIT is a promising, lead-free ferroelectric with a high Curie temperature (T_C ~ 675 °C), a modest spontaneous polarization ~50 μC cm^{-2} and a high coercive field.[18] Apart from applications directly related to their ferroelectricity, BIT nanoparticles are also important in visible-light photocatalysis,[8,11,19] electrocatalysis,[6] and piezocatalysis.[11,19] The hydrothermally synthesized BIT nanoparticles appear in a wide variety of different nano-morphologies, including 2-D platelet crystals, (*i.e.*, rectangular nanoplatelets and nanosheets),[5–7,12,14–16] 1-D crystals (*e.g.*, nanowires, nanobelts, nanobundles, nanorods),[6,7,13,16] and 3-D nanostructures assembled from 1-D or 2-D nanoparticles.[8–11,13,14] The morphology of the formed nanoparticles can be controlled to a large extent by selecting the

[a] *Department for Materials Synthesis, Jožef Stefan Institute, Jamova 39, SI-1000 Ljubljana, Slovenia. E-mail: darko.makovec@ijs.si*
[b] *Jožef Stefan International Postgraduate School, Jamova 39, SI-1000 Ljubljana, Slovenia*

† Electronic supplementary information (ESI) available: List of materials used and additional information on the synthesis and characterization methods, additional TEM and XRD of samples hydrothermally treated in hydroxide of different concentrations and at different temperatures, EDXS elemental maps, STEM analyses, ELNES of Ti-$L_{2,3}$ edge in different bismuth-titanate phases, and TEM of annealed samples. See DOI: https://doi.org/10.1039/d2ce00491g

experimental conditions during the hydrothermal synthesis, *e.g.*, the type and concentration of the mineralizer, the source of titania, the reactant concentrations, the reaction temperature and time, and the use of different surfactants.[6,7,13,15,16] There were several attempts to explain the mechanisms leading to different morphologies, mainly based on the adsorption of the mineralizer cations (Na^+, K^+) on the surfaces of the growing particles[9,13] or templated growth involving layered titanates ($K_2Ti_6O_{13}$, $Na_2Ti_3O_7$) as the templates.[10,15,20]

In our previous paper[16] we revealed that the diverse morphologies of bismuth-titanate nanostructures are related to the different crystalline structures of the formed nanoparticles. In bulk form BIT crystallizes in an Aurivillius layered structure, which is characterized by two structural layers, *i.e.*, a $(Bi_2O_2)^{2+}$ layer and a perovskite $(Bi_2Ti_3O_{10})^{2-}$ layer, alternating along the pseudo-tetragonal *c*-axis.[21] Below the Curie temperature the BIT adopts a monoclinic unit cell (S.G.: *P*1*a*1, a = 5.4449 Å, b = 5.4083 Å, c = 32.8137 Å, β = 89.977°).[22] Because of the layered structure the BIT nanoparticles naturally grow predominantly in the *a*/*b* plane to form rectangular nanoplatelets with the large surfaces parallel to the (001) crystallographic planes. The rectangular BIT nanoplatelets with the Aurivillius-type structure were obtained when the precipitated Bi^{3+} and Ti^{4+} ions were hydrothermally treated for 38 hours at 200 °C in NaOH with a concentration of 2 mol L^{-1}.[16] When the concentration of NaOH was decreased to 0.5 mol L^{-1} the bismuth-titanate nanowires formed.[16] However, structural analyses with a combination of atomic-resolution imaging in a scanning-transmission electron microscope (STEM) and X-ray diffractometry (XRD) showed that the nanowires exhibit a different crystal structure to the nanoplatelets. The structure of the nanowires was explained with an orthorhombic unit cell (a = 3.804 Å, b = 11.816 Å, and c = 9.704 Å). Atomic-resolution, high-angle annular dark-field imaging with a C_S-probe-corrected scanning-transmission electron microscope showed the cation arrangement in two structural layers alternating along the orthorhombic *c*-direction: a structural layer that resembles the $(Bi_2O_2)^{2+}$ layer of the Aurivillius-type structures, and a structural layer composed of two parallel layers of the Ti atoms, where every sixth Ti is replaced by Bi.[16]

In this investigation we systematically analysed the evolution of different crystalline structures/morphologies during the hydrothermal synthesis of BIT. The aim was to reveal the mechanisms involved in the formation of different nanostructures with special attention to the role of metastable polymorphs which appear as the transient phases.

Experimental

The bismuth-titanate nanostructures were synthesized with the hydrothermal treatment of precipitated Bi^{3+} and Ti^{4+} ions. These two ions were precipitated separately. The Bi^{3+} ions were precipitated from a $Bi(NO_3)_3$ aqueous solution with aqueous ammonia, whereas the Ti^{4+} ions were precipitated with addition of water to a *tert*-butanol solution of titanium butoxide. The two precipitates were suspended in mineralizer hydroxide (NaOH or KOH, Bi/Ti = 4/3) and heated in a closed, Teflon-lined autoclave at different temperatures from 80 °C to 220 °C. Details of the synthesis are given in the ESI.†

The products were characterized with transmission electron microscopy (TEM, Jeol 2010F) and a C_S-probe-corrected STEM (Jeol ARM 200CF). XRD patterns were recorded with a PANalytical X' Pert PRO diffractometer (see the ESI† for details).

Results

Influence of the NaOH concentration on the formed phase and morphology

Table 1 summarizes the phase composition and morphology of the product synthesized with the hydrothermal treatment of the suspension of precipitated Ti^{4+} and Bi^{3+} ions suspended in the mineralizer hydroxide under different experimental conditions. Among the tested experimental conditions, the hydroxide concentration had the greatest influence on the formed phase and the morphology of the product particles. The influence of the hydroxide concentration will be demonstrated for the case of a hydrothermal treatment for 38 hours at 200 °C in NaOH. At the lowest tested NaOH concentration of 0.002 mol L^{-1} the product was amorphous (Fig. SI1(a) in the ESI†). The first crystalline product formed at a NaOH concentration of 0.01 mol L^{-1}. With an increasing NaOH concentration the morphology of the crystalline product changed from 1-D particles, *i.e.*, nanowires, at lower NaOH concentrations (0.01 mol L^{-1} to 0.5 mol L^{-1}), over 2-D particles, *i.e.*, nanoplatelets, at medium NaOH concentrations (0.75 mol L^{-1} to 4 mol L^{-1}), to globular particles at the highest NaOH concentrations (8 mol L^{-1} and 12 mol L^{-1}). In the samples treated in NaOH with a concentration of 0.01 mol L^{-1} and 0.1 mol L^{-1}, the nanowires (from 20 to over 100 nm wide and several μm long) were mainly present in the form of large aggregates. Within aggregates the nanowires were crossed at 90° (Fig. SI1(b)† and 1(a)). The selected-area electron diffraction (SAED) pattern taken from the nanowires was consistent with the orthorhombic structure characteristic for bismuth-titanate nanowires[16] (see the inset of Fig. 1(a)). In 0.5 mol L^{-1} NaOH well-separated nanowires (from 15 nm to 35 nm wide and several μm long) formed (Fig. 1(b)). The sample synthesized in 0.75 mol L^{-1} NaOH still contained some shorter nanowires, while the main phase was rectangular platelet crystals (from 200 nm to 500 nm wide and around 50 nm thick) (Fig. SI1(c)†). When the NaOH concentration was further increased to 1 mol L^{-1}, only large (several μm wide) rectangular platelets were formed. The platelets were composed of smaller, rectangular nanoplatelet crystallites. Within each platelet all the crystallites were oriented in nearly the same crystallographic orientation, making a "mosaic" structure (Fig. 1(c)). At NaOH concentrations of 2 mol L^{-1} and 4 mol L^{-1}, much smaller, separated nanoplatelets were synthesized (Fig. 1(d) and SI1(d)†). The nanoplatelets were from 50 nm to 200 nm wide and

Table 1 Phase and morphology of the product obtained with hydrothermal treatment of precipitated Bi^{3+} and Ti^{4+} ions as a function of concentration (c_{OH}) of mineralizer hydroxide, NaOH (N) or KOH (K), temperature (T) and time (t)

		t [h]							
c_{OH} [mol L^{-1}]	T [° C]	0.17	0.5	2	3	6	24	38	72
N 0.002	200							A	
N 0.01	200							AW	
N 0.1	200			A		AW		AW	
N 0.5	200	A	W, A, B	W, PC, B	W, PC	W	W	W	W
N 0.5	80							A	A
N 0.5	100			A, B				A	
N 0.5	140			A, B				W	
N 0.75	200							P, W	
N 1	200			NP@PC, W		NP@PC, W		NP	
N 2	80							A	W, PC, B
N 2	100			A, B				NW, PC, B	
N 2	140			W, PC				NP@PC	
N 2	160			W, PC				NP@PC	
N 2	180			W, PC				NP	
N 2	200	A, B	W, PC, B	W, PC, B	NP@PC, W	NP	NP	NP	NP
N 2	220							NP	
N 4	200							NP	
N 8	200							NP@PC	
N 12	200							PC	
K 0.5	200							AW	
K 2	200	A, B	W, PC, B	W, PC	W, PC	W, PC	W, PC	W, PC	W, PC, P

A···amorphous, B···Bi-based secondary phases ($Bi_2O_2CO_3$, Bi_2O_3), W···nanowires with an orthorhombic structure, AW···aggregated nanowires, PC···globular aggregates of perovskite nanocrystallites, NP···nanoplatelets with an Aurivillius structure, P···larger platelets with an Aurivillius phase, NP@PC···NP growing on the surfaces of PC.

approximately 10 nm thick. The SAED of the nanoplatelets was consistent with the Aurivillius layered-perovskite structure of bismuth titanate.

According to EDXS analysis the nanowires and the nanoplatelets had the same composition, matching that of the starting $Bi_4Ti_3O_{12}$ composition, within the uncertainty of the method. The Na peak was not significant for either of the two morphologies.

At a NaOH concentration of 8 mol L^{-1} the nanoplatelets were growing on the surfaces of larger globular particles (Fig. 1(e)). Finally, at the highest NaOH concentration of 12 mol L^{-1} only globular particles (from 100 nm to 250 nm in size) formed (Fig. 1(f)). Detailed analyses showed that the globular particles were compact aggregates of much smaller crystallites, around 15 nm in size. All the nanocrystallites making up an individual globular particle were oriented in a similar crystallographic orientation, resulting in a single-crystal-like SAED pattern with diffuse, streaked reflections corresponding to a (quasi)cubic unit cell with a = ~3.9 Å (insets of Fig. 1(e) and (f), see also the dark-field (DF) TEM image, Fig. SI2†).

Fig. 2 shows the XRD patterns of the samples synthesized in NaOH with an increasing concentration. The nanowires exhibited an orthorhombic structure characteristic for the bismuth-titanate nanowires[16] (see patterns (a) and (b) for the samples synthesized in 0.1 mol L^{-1} NaOH and 0.5 mol L^{-1} NaOH, respectively). The structure is different to the Aurivillius structure of the bismuth-titanate nanoplatelets (see patterns (c) and (d) for the samples synthesized in 1 mol L^{-1} NaOH and 2 mol L^{-1} NaOH, respectively). Detailed structural analyses of the nanoplatelets and the nanowires are given in ref. 16. The XRD pattern of the sample synthesized in 12 mol L^{-1} NaOH consisted of sharp reflections corresponding to two Bi-rich phases, *i.e.*, $Bi_2O_2CO_3$ (PDF #004-0666) and Bi_2O_3 (PDF #006-0294), and broad reflections at the positions consistent with the quasi-cubic cell. Most probably, the $Bi_2O_2CO_3$ formed from the reaction between the nanoparticles obtained with the precipitation of Bi^{3+} ions and the atmospheric carbon dioxide dissolved in the water.[23]

The electron and X-ray diffractions of the globular aggregates match well with the perovskite structure. Sodium bismuth titanate ($Bi_{0.5}Na_{0.5}TiO_3$) perovskite is known to form during a hydrothermal treatment at high NaOH concentrations.[9,17] However, the EDXS analysis in the TEM showed that the globular aggregates contained a much lower concentration of Na than expected for the stoichiometric $Bi_{0.5}Na_{0.5}TiO_3$. According to the EDXS analysis, the globular aggregates synthesized in 12 mol L^{-1} NaOH contained approximately 20 at% of Ti, 12.5 at% of Bi, and 3–6 at% of Na. Here it should be noted that the quantitative EDXS analysis is limited by the bismuth's evaporation under electron-beam irradiation, non-ideal particle morphologies and the possible migration of the sodium atoms from the analysis site. The composition of the sample was also verified with chemical analysis. Even though the sample contained some Bi-rich secondary phases, the Na/Ti ratio measured with ICP-AES analysis[16] confirmed the Na deficiency

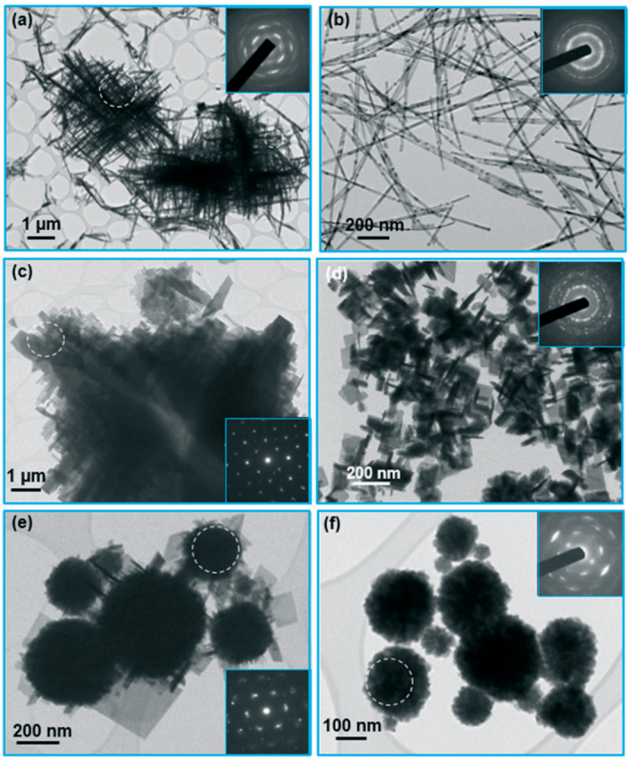

Fig. 1 TEM images with corresponding electron-diffraction patterns (the area where the pattern was recorded is marked with a white circle) of the product synthesized by hydrothermal treatment of precipitated Ti^{4+} and Bi^{3+} ions for 38 hours at 200 °C in NaOH of increasing concentration: (a) 0.1 mol L^{-1}, (b) 0.5 mol L^{-1}, (c) 1 mol L^{-1}, (d) 2 mol L^{-1}, (e) 8 mol L^{-1}, and (f) 12 mol L^{-1}.

suggested by the EDXS. Most probably, the excess charge expected due to the excess of Bi^{3+} ions over the Na^{+} ions at the A sites of the ABO_3 perovskite structure is compensated by charged cationic vacancies.

In summary, the single-phase bismuth-titanate nanowires and nanoplatelets are obtained with the hydrothermal treatment of precipitated Bi^{3+} and Ti^{4+} ions in NaOH with concentration of 0.5 mol L^{-1} and 2 mol L^{-1}, respectively.

Formation of bismuth-titanate nanoplatelets

To reveal the mechanisms involved in the formation of different nanostructures we followed the phase evolution with the temperature and time of the hydrothermal treatment. First, we present the formation of the nanoplatelets in 2 mol L^{-1} NaOH, as the platelet shape of the crystals is characteristic of the compounds with a layered Aurivillius-type structure. Both ions, *i.e.*, Ti^{4+} and Bi^{3+}, precipitated at room temperature in the form of agglomerated amorphous nanoparticles (Fig. SI3†). However, after the precipitates were admixed into the NaOH solution, the amorphous bismuth hydroxide nanoparticles grew to micron-sized, needle-like crystals at room temperature (Fig. SI3(c)†). Fig. 3 shows the XRD patterns of the product obtained with hydrothermal treatment of the precipitated ions for different times at 200 °C, whereas Fig. 4 shows the corresponding TEM images. After 10 minutes at 200 °C, some Bi-based needle-like crystals remained in the product. The rest of the product consisted of amorphous nanoparticles (Fig. 4(a)). Frequently, the nanoparticle agglomerates had a spherical shape (marked with a circle in Fig. 4(a)). The primary nanoparticles within the agglomerates exhibited two distinct morphologies: apart from globular nanoparticles (~5 nm in size), some elongated nanoparticles (~4 nm wide and up to 100 nm long) were present (Fig. 4(b)). It was not

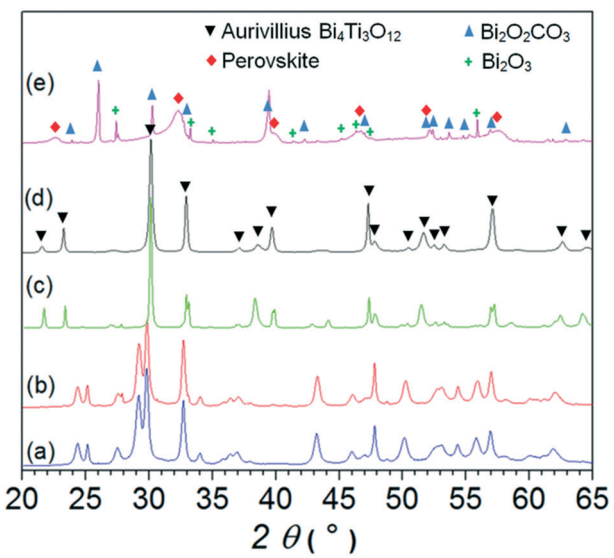

Fig. 2 XRD patterns of samples synthesized with hydrothermal treatment for 38 h at 200 °C in NaOH with different concentrations: (a) 0.1 mol L^{-1} NaOH, (b) 0.5 mol L^{-1} NaOH, (c) 1 mol L^{-1} NaOH, (d) 2 mol L^{-1} NaOH, and (e) 12 mol L^{-1} NaOH.

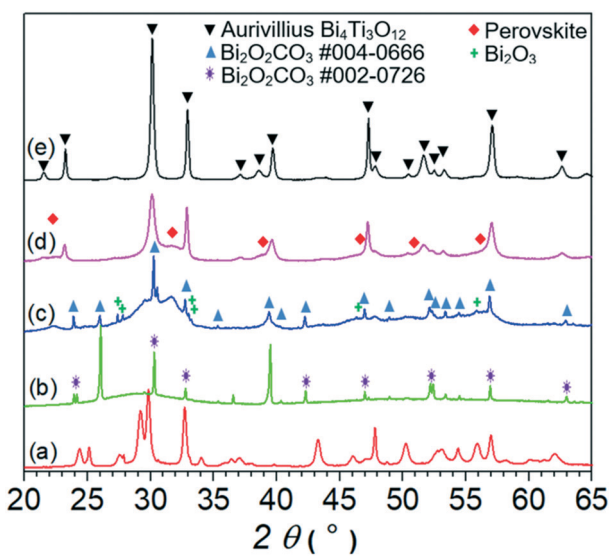

Fig. 3 XRD patterns of nanowires hydrothermally synthesized with treatment for 38 h at 200 °C in 0.5 mol L^{-1} NaOH (a) and samples treated for different times at 200 °C in 2 mol L^{-1} NaOH: 10 minutes (b), 1 hour (c), 3 hours (d), and 38 hours (e).

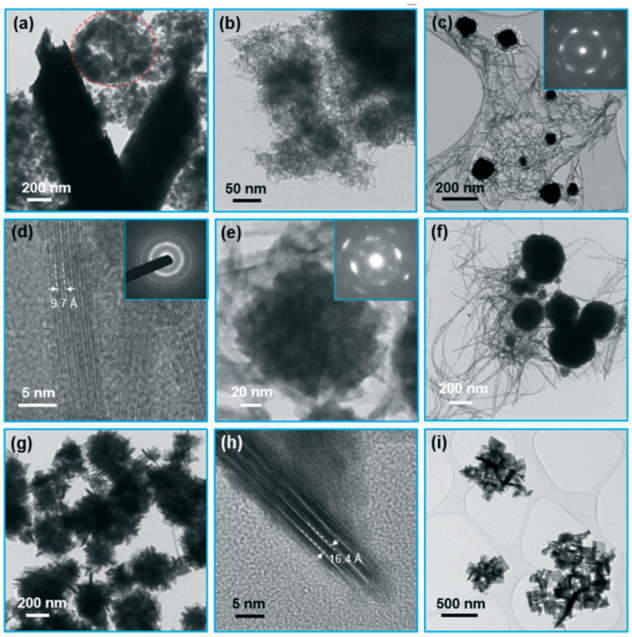

Fig. 4 TEM images of product nanoparticles after hydrothermal treatment for different times at 200 °C in 2 mol L^{-1} NaOH: (a) and (b) 10 minutes, (c) 0.5 hour (inset: SAED pattern recorded from a globular aggregate marked with a circle), (d) HRTEM image of the nanowire in the sample treated for 0.5 hour (inset: SAED pattern of the area with nanowires), (e) TEM image with a corresponding SAED pattern of the globular nanoparticle aggregate in the product after 1 hour, (f) 2 hours, and (g) 3 hours, (h) HRTEM image of the nanoplatelet at the surface of the globular aggregate after 3 hours and (i) 12 hours.

possible to resolve whether the nanoparticles with the two morphologies exhibit different compositions, because analyses at higher resolutions were not possible due to radiation damage. The XRD pattern of the product treated for 10 minutes consisted of sharp reflections, which can be ascribed to two modifications of $Bi_2O_2CO_3$ (PDF #004-0666, PDF #002-0726) protruding from broad "humps" of the almost amorphous phase (Fig. 3, see pattern (b)).

When the time of the hydrothermal treatment at 200 °C was prolonged to 30 minutes, Bi-based crystals were still sometimes observed with the TEM. However, most of the product consisted of particles having two different morphologies: nanowires (3–10 nm wide and up to ~200 nm long) and larger globular particles (from ~30 nm to over 200 nm in size) (Fig. 4(c)). The SAED pattern taken from the nanowires was consistent with the orthorhombic structure of bismuth-titanate nanowires[16] (see the inset of Fig. 4(d)). High-resolution TEM (HRTEM) images (Fig. 4(d)) confirmed the single-crystalline nature of the nanowires. The dominant periodicity across the nanowire shown in Fig. 4(d) of 9.7 Å corresponds to the (001) planes of its orthorhombic structure. The globular particles were dense aggregates of smaller crystallites (a few nm in size) with a quasi-cubic structure, similar to the globular particles in the sample treated for 38 hours in 12 mol L^{-1} NaOH (see Fig. 1(f)). The crystallites constituting an individual aggregate were all oriented in a similar crystallographic orientation (see insets of Fig. 4(c) and (e)). After 1 hour, and also after 2 hours, of the treatment at 200 °C the product was similar to that after 30 minutes, only the size of both types of product particles gradually increased (Fig. 4(f)). XRD patterns of the products treated at 200 °C for 1 hour and 2 hours showed sharp reflections corresponding to the unreacted Bi-rich phases, *i.e.*, $Bi_2O_2CO_3$ and Bi_2O_3 (PDF #006-0294), and broad reflections (Fig. 2, pattern (c)). The broad reflections were located at the positions where the pure nanowires exhibited high-intensity reflections (see Fig. 2, pattern (a)) and at the positions consistent with the quasi-cubic unit cell with a = ~3.9 Å.

A large change in the morphology of product particles occurred when the treatment time was increased to 3 hours. The nanowires almost completely disappeared, while on the surfaces of the globular aggregates well-defined rectangular nanoplatelets grew (Fig. 4(g)). Fig. 4(h) shows the lattice image of a nanoplatelet growing on the surface of an aggregate. The nanoplatelet is oriented with its large surfaces parallel to the electron beam. The dominant periodicity of the fringes across the nanoplatelet of 16.4 Å corresponds to the (002) planes of the Aurivillius $Bi_4Ti_3O_{12}$ structure. The corresponding XRD pattern (Fig. 3, pattern (d)) exhibits reflections corresponding to the Aurivillius structure and broad reflections of the quasi-cubic phase. With further prolongation of the treatment at 200 °C the nanowires and the quasi-cubic phase disappeared completely while the nanoplatelets grew. At first, the nanoplatelets remained in the form of small, distinct agglomerates, reflecting their formation with growth from the individual globular aggregate (Fig. 4(i)). Only after approximately 24 hours did the nanoplatelets separate. A TEM image and an XRD pattern of the final sample treated for 38 hours are shown in Fig. 1(d) and 2(pattern (d)), respectively. Also, after treatment for 3 days at 200 °C the product remained in the form of nanoplatelets of similar size compared to that after 38 hours.

The evolution of the nanoplatelets was also monitored with the treatment temperature. Short nanowires were obtained after treatment for a long time (3 days) at 80 °C (Fig. SI4†). After the treatment for 2 hours at 100 °C the product was composed of amorphous nanoparticles (Fig. SI5(a)†), similar to the sample treated for 10 minutes at 200 °C, whereas after 38 h at 100 °C the material was composed of globular nanocrystalline aggregates and nanowires (Fig. SI5(b)†). At 140 °C the product was composed of globular aggregates and nanowires after 2 hours, whereas after 38 hours the product was composed of globular aggregates with nanoplatelets growing from their surfaces (Fig. SI6†), similar to the sample treated for 3 hours at 200 °C. Also, the samples treated for 2 hours at 160 °C and 180 °C contained a mixture of globular aggregates and nanowires, whereas after 38 hours the sample treated at 160 °C contained a mixture of aggregated nanoplatelets and some larger globular aggregates with nanoplatelets growing from their surfaces (Fig. SI7†) and the sample treated at 180 °C contained only nanoplatelets (Fig. SI8†). Also, at the highest temperature of 220 °C only nanoplatelets were obtained.

The nature of the globular aggregates of nanocrystallites with the quasi-cubic structure

The presented analyses showed that the nanoplatelets with an Aurivillius structure always grow on the surfaces of the globular aggregates of nanocrystals with a quasi-cubic structure. The diffraction patterns of the globular aggregates matched with the perovskite structure. Unfortunately, the aggregates were too large (the object was too thick) for the atomic-resolution STEM imaging. However, when the reaction suspension was intensely stirred during the hydrothermal treatment, the aggregation of the nanocrystals was impeded and a part of the formed quasi-cubic nanocrystallites remained loosely agglomerated. High-angle annular dark-field (HAADF) STEM imaging of the loosely agglomerated nanocrystallites showed poor structural order; however, locally the atomic structure matched with the perovskite structure (see the ESI,† Fig. SI9). However, the EDXS analysis of the globular aggregates showed no Na, only Bi and Ti in a ratio roughly matching the starting $Bi_4Ti_3O_{12}$ composition within the uncertainty of the method. The result of the EDXS analysis was confirmed with ICP-OES chemical analysis.[16] The sample hydrothermally treated for 1 hour at 200 °C contained less than 0.2 wt% of Na.

The absence of Na^+ raises a question about the valence of Ti in the perovskite structure. The Ti valence can be determined from electron-energy-loss spectroscopy (EELS) as the energy-loss near-edge structure (ELNES) of the Ti-$L_{2,3}$ edge depends on the valence of Ti if the atomic environment of the ions remains unchanged. The Ti-$L_{2,3}$ ELNES shows a clear four-peak feature for Ti^{4+}, whereas for Ti^{3+} the two peaks featuring both L_2 and L_3 merge into one peak when the energy resolution is limited.[24,25] The Ti-$L_{2,3}$ ELNES was identical for different bismuth-titanate particles and matched the ELNES for the Ti^{4+} standard, strongly suggesting the 4+ oxidation state of Ti in all three morphologies, *i.e.*, the nanoplatelets, the nanowires and the perovskite nanocrystallites (see the ESI† for details; Fig. SI10). The 4+ oxidation state of Ti is also consistent with the white colour of the powders (Ti^{4+} has no d-electrons). A significant amount of Ti^{3+} (one d-electron) would result in an intense dark colour.[26]

The transformation from the perovskite phase to the Aurivillius phase

The transformation from the quasi-cubic phase to the Aurivillius phase was studied using atomic-resolution STEM imaging. Fig. 5 shows the STEM images of a nanoplatelet growing from a globular aggregate of the quasi-cubic phase. The nanoplatelet is oriented along the $[110]_{AU}$ direction of its Aurivillius structure. In the "Z-contrast" HAADF images the intensity of the spots representing an individual atomic column depends on the column's average atomic number Z ($\sim Z^{\alpha}$ with α slightly lower than 2).[27] The columns containing the heavier Bi^{3+} ions appear much brighter than the columns containing the Ti^{4+} ions, while the O^{2-} ions are too light to be detected. Thus, the spots can be directly related to the positions of the different columns of the structure. In the HAADF images of the nanoplatelet the two layers of the Aurivillius $Bi_4Ti_3O_{12}$ structure, *i.e.*, a $(Bi_2O_2)^{2+}$ layer and a $(Bi_2Ti_3O_{10})^{2-}$ perovskite-like layer, can be clearly distinguished. The nanoplatelets exhibit a regular structure with few defects. In particular, the dimension of the perovskite layer is sometimes enlarged: instead of the $(Bi_2Ti_3O_{10})^{2-}$ composition (two layers of Bi ions) the defected perovskite layer shows the $(Bi_3Ti_4O_{13})^{2-}$ composition (three layers of Bi ions marked with an arrow in Fig. 5(b)). Interestingly, the nanoplatelets' structure always terminates at the large {001} surfaces with the $(Bi_2O_2)^{2+}$ layers. The nanoparticles with layered structures, such as the Aurivillius-type structure, will normally terminate at the surfaces with a specific, low-energy atomic layer.[28] The nanoplatelet epitactically grows from the perovskite aggregate. In the vicinity of the nanoplatelets the perovskite contains individual $(Bi_2O_2)^{2+}$ layers, characteristic for the Aurivillius structure (marked with magenta lines in Fig. 5(c)), suggesting a gradual transformation with ordering of the two cations within the defected perovskite structure.

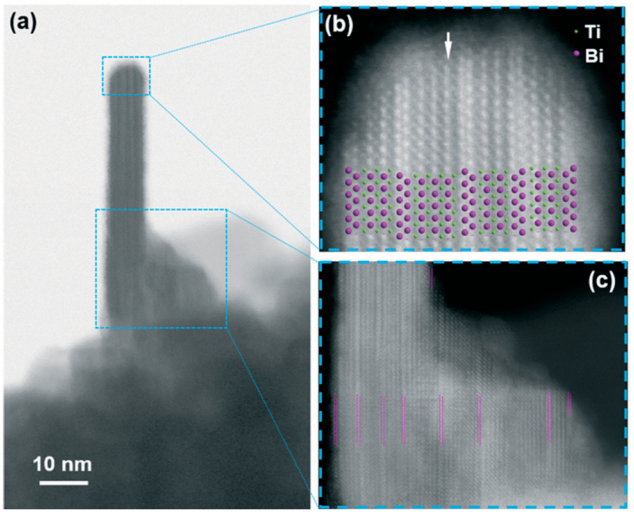

Fig. 5 BF (a) and HAADF ((b) and (c)) STEM images of the bismuth-titanate nanoplatelet growing on the surface of the nanoparticle aggregate. (a) and (b) The model of the Aurivillius structure projected along the $[110]_{AU}$ direction is superimposed over the image (b) to illustrate the positions of the Bi^{2+} and Ti^{4+} ions. Double magenta lines in Fig. 5(c) show the position of the $(Bi_2O_2)^{2+}$ structural layers.

Formation of bismuth-titanate nanowires

When the treatment occurred in NaOH with a concentration of 0.5 mol L^{-1}, the morphology of the formed particles evolved in a remarkably different way compared to the higher NaOH concentration (2 mol L^{-1}). After 30 minutes at 200 °C the product consisted of a mixture of short nanowires and globular nanoparticles with sizes of approximately 5–15 nm. The globular nanoparticles were dispersed between the nanowires or they formed agglomerates. The larger agglomerates of nanoparticles (up to 1 μm in size) usually had a round shape (Fig. 6(a)). The EDXS analysis showed a similar composition for

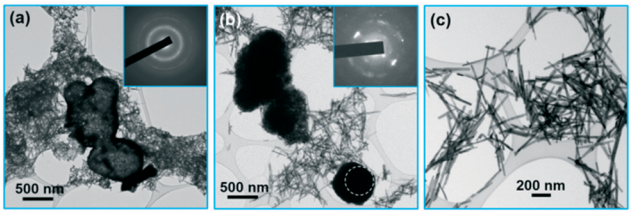

Fig. 6 TEM images of product nanoparticles after hydrothermal treatment for different times at 200 °C in 0.5 mol L^{-1} NaOH: (a) after 0.5 hour, (b) after 3 hours, and (c) after 6 hours.

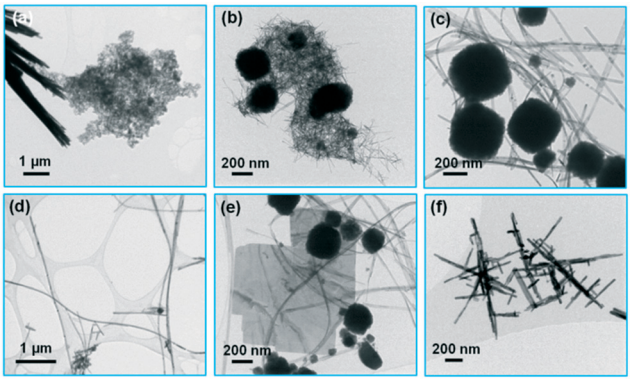

Fig. 7 Product nanoparticles after hydrothermal treatment for different times at 200 °C in KOH: (a) 10 minutes in 2 mol L^{-1} KOH, (b) 1 hour in 2 mol L^{-1} KOH, (c) and (d) 38 hours in 2 mol L^{-1} KOH, (e) 3 days in 2 mol L^{-1} KOH, and (f) 38 hours in 0.5 mol L^{-1} KOH.

both the morphologies of the nanoparticles (EDXS elemental mapping is given in the ESI,† Fig. SI11). The SAED pattern recorded on the nanowires (the inset of Fig. 6(a)) matched with the orthorhombic structure, while the electron diffraction of the globular nanoparticles showed their amorphous nature. With the prolongation of the treatment time to 1 hour the composition and the morphology of the product remained almost unchanged. Only after 2 hours at 200 °C did the product change significantly. The smaller agglomerates of globular nanoparticles disappeared, while the larger agglomerates compacted into dense globular aggregates. The SAED recorded from the aggregates showed patterns composed of diffuse reflections matching with the perovskite structure of numerous small nanocrystallites, all oriented in a similar direction within the individual aggregate (Fig. 6(b)). Bi-Based particles were also sometimes found in the samples treated up to 3 hours. However, the amounts of these unreacted phases were low, as the XRD analysis only showed very broad reflections at the positions of the orthorhombic structure of the nanowires, which become much sharper with the treatment time (Fig. SI12†). After 6 hours at 200 °C the product was composed of nanowires, approximately 20 nm wide and up to 1 μm long (Fig. 6(c)). Only very rarely were large nanocrystalline globular aggregates of perovskite nanocrystallites still found.

The morphology of the formed nanoparticles evolved in a different way in 0.5 mol L^{-1} NaOH also with the treatment temperature, when compared with the treatment in 2 mol L^{-1} NaOH. A very long treatment (3 days) at 80 °C resulted in the formation of globular amorphous nanoparticles with a bimodal size distribution: the smaller were approximately 10 nm and the larger approximately 200 nm in size (Fig. SI13†). The EDXS analysis showed the same composition for the two sizes, roughly matching the starting $Bi_4Ti_3O_{12}$ composition. The amorphous globular nanoparticles, partially agglomerated into round aggregates, also formed after 2 hours at 100 °C (Fig. SI14(a)†) and at 140 °C (Fig. SI15(a)†). After 38 hours the amorphous globular nanoparticles were present at 100 °C (Fig. SI14(b)†), whereas at 140 °C and above only nanowires formed (Fig. SI15(b)†).

The influence of the type of mineralizer hydroxide

Besides the hydroxide concentration, the type of hydroxide has a large effect on the hydrothermal synthesis of bismuth titanate. When KOH was used as the mineralizer at the higher concentration of 2 mol L^{-1}, the evolution of the phases with the treatment time at 200 °C started like that with NaOH. After 10 minutes, only unreacted Bi-based large crystals and amorphous product nanoparticles were present (Fig. 7(a)). After 1 hour, a mixture of nanowires and globular perovskite aggregates formed, as with NaOH (Fig. 7(b)). However, with further prolongation of the treatment time the nanowires grew, while the globular aggregates remained almost unchanged. Thus, after 38 hours at 200 °C the mixture of globular aggregates and nanowires was synthesized (Fig. 7(c)). The individual nanowires were extremely long, exceeding 15 μm (Fig. 7(d)). Only after a very long time (3 days) at 200 °C did large platelets of the Aurivillius phase appear in the mixture of nanowires and globular aggregates (Fig. 7(e)).

At the lower KOH concentration of 0.5 mol L^{-1}, only aggregated nanowires formed with the treatment for 38 hours at 200 °C. Similar to the product synthesized in 0.1 mol L^{-1} NaOH, the nanowires were usually intergrown at an angle of 90° (Fig. 7(f)).

Discussion

Three different crystalline bismuth-titanate phases form during the hydrothermal treatment of the precipitated Ti^{4+} and Bi^{3+} ions in hydroxide, each characterized by a specific morphology, *i.e.*, the nanowires with an orthorhombic structure, the quasi-cubic perovskite phase in the form of globular aggregates of nanocrystallites, and the nanoplatelets with an Aurivillius layered-perovskite structure. The formation of bismuth titanate always starts with the formation of amorphous nanoparticles composed of Bi, Ti and O. With the increasing temperature, the amorphous nanoparticles crystallize into the nanowires and the aggregates of perovskite nanocrystallites. It seems that the crystallization is influenced by the aggregation of the amorphous nanoparticles. Namely, a part of the amorphous nanoparticles assembled into compact globular aggregates prior to the crystallization (Fig. 3(a)). It is likely that the aggregated

amorphous nanoparticles crystallize into the perovskite, while the nanowires are formed from the dispersed amorphous nanoparticles. As the surface energy has a significant contribution to the thermodynamics of the nanoparticles, the state of agglomeration can determine the formed modification. A well-known example is the formation of iron-oxide nanoparticles. Maghemite (γ-Fe_2O_3) is formed when the nanoparticles crystallize in the agglomerated state, whereas ε-Fe_2O_3 forms when the nanoparticles grow confined in a silica matrix.[29]

The Aurivillius $Bi_4Ti_3O_{12}$ nanoplatelets always formed with growth at the surfaces of the perovskite nanocrystalline aggregates. The perovskite forms as a transient phase during the formation of the Aurivillius phase. The formation of the perovskite nanocrystals is faster than the formation of the ordered layered-perovskite Aurivillius phase. Thus, the perovskite forms first and only with ordering of the ions within the perovskite structure and the Aurivillius platelet crystals nucleate and grow at the surfaces of the perovskite aggregates.

From the thermodynamics point of view, only the Aurivillius $Bi_4Ti_3O_{12}$ is stable, whereas the orthorhombic nanowires and the perovskite are "metastable" polymorphs. According to the empirical Ostwald step rule, a thermodynamically unstable polymorph often occurs before the stable phase, because it has a lower energy barrier for nucleation during the crystallization than the stable phase.[30,31] It usually transforms in an energetically cascading series of polymorphic stages to the equilibrium phase. However, if the unstable polymorph has a lower surface energy than the equilibrium polymorph it can remain stable at the nanoscale.[31] Metastable polymorphs of simple oxides stabilized at the nanoscale represent some of the technologically most important nanomaterials, *e.g.*, photocatalytic anatase and magnetic maghemite nanoparticles. However, the metastable polymorphs are not restricted to simple oxides. Recently, we presented a metastable polymorph of magnetic strontium hexaferrite ($SrFe_{12}O_{19}$) stabilized at the nanoscale.[32] With growth, *e.g.*, during annealing at high temperatures, such metastable polymorph nanoparticles will transform to the thermodynamically stable phase. The bismuth-titanate nanowires topotactically transform to the equilibrium Aurivillius structure with annealing at temperatures above 500 °C.[16] Also, annealing of the perovskite aggregates resulted in the transformation to the Aurivillius phase. For example, annealing of the perovskite aggregates in the sample treated in 2 mol L^{-1} NaOH for 1 hour at 200 °C resulted in the transformation to the Aurivillius phase (see the ESI† for details, Fig. SI16).

We were not able to accurately measure the chemical composition of the three phases. However, the absence of any precipitation of secondary phases during the transformations between the different phases strongly suggests that they all have the same composition. For example, no precipitation of any secondary phase was observed during the topotactic transformation from the orthorhombic nanowire structure to the Aurivillius structure.[16] Also, no secondary phase was detected after the epitaxial growth of the Aurivillius nanoplatelets on the surfaces of the nanocrystalline perovskite aggregates (see Fig. 5).

The composition with a Bi/Ti atomic ratio of 4/3 is particularly strange for the perovskite. This suggests a high concentration of vacancies at the octahedral B sites of the ABO_3 perovskite structure $\left(Bi^{3+}Ti^{4+}_{0.75}(V''''_{Ti})_{0.25}O_3\right)$. The titanium vacancies are known to be the equilibrium charged defects formed for the compensation of excess charge during donor incorporation into some perovskite titanates, such as $BaTiO_3$.[33] For example, in the bulk ceramics at 1400 °C in air, up to ~30 mol% of La^{3+} donors can be incorporated into the $BaTiO_3$ structure at the Ba sites with the simultaneous formation of titanium vacancies for the charge compensation $\left(Ba^{2+}_{0.70}La^{3+}_{0.30}Ti^{4+}_{0.925}(V''''_{Ti})_{0.075}O_3\right)$.[34] For the bulk materials, the concentration of (V''''_{Ti}) required for the charge balance in the perovskite with the starting $BiTi_{0.75}O_3$ composition seems unrealistically high. However, the perovskite phase obtained by the hydrothermal treatment was always in the form of (aggregated) nanocrystallites, where the large flexibility of the structure and the composition can be expected.[35] The concentration of the charged vacancies required to maintain the charge neutrality can be decreased with the partial reduction of Ti^{4+} to Ti^{3+}, accompanied by precipitation of the excess Bi^{3+}. However, the EELS analysis (Fig. SI10†) and the white colour of the powders suggested the Ti was present in the oxidation state 4+.

The stability of different phases depends decisively on the hydroxide concentration. Independent of the hydroxide concentration, the nanowires and the globular aggregates of perovskite nanocrystallites form with the crystallization of the amorphous nanoparticles in the initial stages of hydrothermal treatment. However, at higher concentrations ($\geq$1 mol L^{-1} NaOH) the perovskite aggregates further transform into the Aurivillius nanoplatelets, while the nanowires dissolve. In contrast, at lower concentrations ($\leq$1 mol L^{-1} NaOH), the nanowires grow with the treatment temperature/time, while the perovskite aggregates dissolve.

The kinetics of hydrothermal reactions during the synthesis of bismuth titanate evidently increases with the concentration of mineralizer hydroxide. At a higher NaOH concentration (2 mol L^{-1}) the first crystalline particles form at 80 °C, below the boiling point of the aqueous reaction suspension, provided that the treatment time is long enough. That is a considerably lower temperature than at the lower concentration (0.5 mol L^{-1}), where the first crystalline phases appeared above 100 °C. The kinetics also depends on the type of mineralizer hydroxide, with faster kinetics in NaOH than in KOH. The kinetics of the hydrothermal reactions further defines the morphology of the formed nanostructures. At NaOH concentrations of 2 mol L^{-1} and 4 mol L^{-1} the fast kinetics of the perovskite-to-Aurivillius transformation leads to a high nucleation rate and the formation of small nanoplatelets (Fig. 1(d)). In 1 mol L^{-1} NaOH the transformation kinetics is slower, leading to a lower

nucleation rate and a higher growth rate, resulting in the rapid growth of the Aurivillius phase into much larger platelet crystals (Fig. 1(c)) than in 2 mol L^{-1} NaOH. Similarly, the nucleation of nanowires is faster in 0.5 mol L^{-1} NaOH than in 0.1 mol L^{-1} and 0.01 mol L^{-1} of NaOH, resulting in smaller, individual nanowires (Fig. 1(b)). At lower concentrations the slower nucleation rate and the faster growth rate result in rapid growth, leading to larger, crossed nanowires (Fig. 1(a)).

Conclusions

The formation of bismuth-titanate nanoplatelets and nanowires during the hydrothermal treatment of precipitated Bi^{3+} and Ti^{4+} ions in the mineralizer hydroxide was systematically studied by a combination of X-ray diffractometry and transmission and scanning-transmission electron microscopies. The nanowires with a specific orthorhombic structure form at lower NaOH concentrations ($\leq$1 mol L^{-1}), whereas nanoplatelets with an Aurivillius layered-perovskite structure form at higher NaOH concentrations ($\geq$1 mol L^{-1}) when the precipitated ions are hydrothermally treated for a long time (38 hours) at 200 °C. At an even higher NaOH concentration (>8 mol L^{-1}), sodium incorporates into the structure, leading to the formation of aggregated perovskite nanocrystallites.

The formation of both bismuth-titanate nanostructures, *i.e.*, the orthorhombic nanowires and the Aurivillius nanoplatelets, starts with crystallization from amorphous nanoparticles. The subsequent phase (and morphology) evolution depends on the concentration of hydroxide, which influences the stability of different phases and the kinetics of the hydrothermal reactions. The reaction kinetics increases with the hydroxide concentration. Independent of the hydroxide concentration, the nanowires and globular aggregates of the perovskite nanocrystallites form in the initial stage of the hydrothermal synthesis. The highly defected perovskite nanocrystallites contain Bi^{3+} and Ti^{4+} cations (significant amounts of Na^{+} or Ti^{3+} could not be detected). At lower NaOH concentrations the nanowires grow with the treatment temperature/time, while the perovskite aggregates dissolve. At higher NaOH concentrations the nanowires dissolve, while the Aurivillius nanoplatelets epitaxially grow on the surfaces of the perovskite nanocrystalline aggregates. A change of NaOH for KOH decreases the reaction kinetics and favours the formation of nanowires.

Conflicts of interest

There are no conflicts to declare.

Acknowledgements

The authors acknowledge the financial support from the Slovenian Research Agency (ARRS) for research core funding No. P2-0089.

References

1 I. I. Naumov, L. Bellaiche and H. X. Fu, *Nature*, 2004, **432**, 737–740.
2 H. Li, L. Su, S. Kuang, Y. Fan, Y. Wu, Z. L. Wang and G. Zhu, *Nano Res.*, 2017, **10**, 785–793.
3 Y. Garbovskiy and A. Glushchenko, *Nanomaterials*, 2017, **7**, 361-1–361-20.
4 C.-C. Wang, F.-C. Li, R.-J. Wu, V. A. Hovhannisyan, W.-C. Lin, S.-J. Lin, P. T. C. So and C.-Y. Dong, *J. Biomed. Opt.*, 2009, **14**, 044034-1–044034-4.
5 Q. Yang, Y. Li, Q. Yin, P. Wang and Y.-B. Cheng, *J. Eur. Ceram. Soc.*, 2003, **23**, 161–166.
6 Z. Chen, Y. Yu, H. Guo and J. Hu, *J. Phys. D: Appl. Phys.*, 2009, **42**, 125307-1–125307-9.
7 J. Hu, Y. Yu, H. Guo, Z. Chen, A. Li, X. Feng, B. Xi and G. Hu, *J. Mater. Chem.*, 2011, **21**, 5352–5359.
8 L. Xue, G. Qing-Feng, L. Hai-Bo, L. Hong-Ji, B. Chun-Hua and D. Hai-De, *Acta Phys.-Chim. Sin.*, 2012, **28**, 1481–1488.
9 S. Tu, H. Huang, T. Zhang and Y. Zhang, *Appl. Catal., B*, 2017, **219**, 550–562.
10 J. Wu, N. Qin, E. Lin, B. Yuan, Z. Kang and D. Bao, *Nanoscale*, 2019, **11**, 21128–21136.
11 S. Niu, R. Zhang, X. Zhang, J. Xiang and C. Guo, *Ceram. Int.*, 2020, **46**, 6782–6786.
12 H. Gu, Z. Hu, Y. Hu, Y. Yuan, J. You and W. Zou, *Colloids Surf., A*, 2008, **315**, 294–298.
13 F. Wang, J. Wang, X. Zhong, B. Li, J. Liu, D. Wu, D. Mo, D. Guo, S. Yuan, K. Zhang and Y. Zhou, *CrystEngComm*, 2013, **15**, 1397–1403.
14 F. Wang, J. B. Wang, X. L. Zhong, B. Li, Y. Zhang, C. J. Lu, W. N. Ye and Y. C. Zhou, *EPL*, 2013, **103**, 37002-1–37002-6.
15 G. Xu, Y. Yang, H. Bai, J. Wang, H. Tian, R. Zhao, X. Wei, X. Yang and G. Han, *CrystEngComm*, 2016, **18**, 2268–2274.
16 D. Makovec, N. Križaj, A. Meden, G. Dražić, H. Uršič, R. Kostanjšek, M. Šala and S. Gyergyek, *Nanoscale*, 2022, **14**, 3537–3544.
17 R. Lu, J. Yuan, H. Shi, B. Li, W. Wang, D. Wang and M. Cao, *CrystEngComm*, 2013, **15**, 3984–3991.
18 A. Moure, *Appl. Sci.*, 2018, **8**, 62-1–62-16.
19 T. Xiao, C. Guo, H. Wanga, R. Zhang, Y. Li, W. Shao, Y. Zhang, X. Wu, J. Tan and W. Ye, *Mater. Lett.*, 2020, **269**, 127679-1–127679-4.
20 P. Hao, Z. Zhao, J. Tian, Y. Sang, G. Yu, H. Liu, S. Chen and W. Zhou, *Acta Mater.*, 2014, **62**, 258–266.
21 B. Aurivillius, *Ark. Kemi*, 1949, **1**, 499–512.
22 D. Urushihara, M. Komabuchi, N. Ishizawa, M. Iwata, K. Fukuda and T. Asaka, *J. Appl. Phys.*, 2016, **120**, 142117-1–142117-5.
23 J. L. Ortiz-Quiñonez, C. Vega-Verduga, D. Díaz and I. Zumeta-Dubé, *Cryst. Growth Des.*, 2018, **18**, 4334–4346.
24 Y. Shao, C. Maunders, D. Rossouw, T. Kolodiazhnyi and G. A. Botton, *Ultramicroscopy*, 2010, **110**, 1014–1019.
25 L. Lin, Y. Ma, J. Wu, F. Pang, J. Ge, S. Sui, Y. Yao, R. Qi, Y. Cheng, C.-G. Duan, J. Chu and R. Huang, *J. Phys. Chem. C*, 2019, **123**, 20949–20959.

26 R. J. D. Tilley, Transition-Metal Ion Colors, in *Encyclopedia of Color Science and Technology*, ed. R. Luo, Springer, New York, NY, 2013.
27 A. C. T. Koch, Determination of Core Structure Periodicity and Point Defect Density along Dislocations, *Ph.D. Thesis*, Arizona State University, 2002.
28 D. Makovec, B. Belec, T. Goršak, D. Lisjak, M. Komelj, G. Dražić and S. Gyergyek, *Nanoscale*, 2018, **10**, 14480–14491.
29 M. Gich, A. Roig, E. Taboada, E. Molins, C. Bonafos and E. Snoeck, *Faraday Discuss.*, 2007, **136**, 345–354.
30 I. N. Stranski and D. Totomanow, *Z. Phys. Chem.*, 1933, **163**, 399–408.
31 A. Navrotsky, *Proc. Natl. Acad. Sci. U. S. A.*, 2004, **101**, 12096–12101.
32 D. Makovec, G. Dražić, S. Gyergyek and D. Lisjak, *CrystEngComm*, 2020, **22**, 7113–7122.
33 D. M. Smyth, *J. Electroceram.*, 2002, **9**, 179–186.
34 D. Makovec, Z. Samardžija, U. Delalut and D. Kolar, *J. Am. Ceram. Soc.*, 1995, **78**, 2193–2197.
35 D. Makovec and M. Drofenik, *J. Nanopart. Res.*, 2008, **10**, 131–141.